Photochemistry and Photobiology, 20**, **: *–*

Research Article

Toward a Holistic Understanding and Models of Nonphotochemical Quenching Effects on *In Vivo* Fluorometry of Chlorophyll *a* in Coastal Waters

Yuyuan Xie*,†, Gary H. Wikfors, Mark S. Dixon, Lisa Guy, Melissa Krisak and Yaqin Li

Milford Laboratory, NOAA, Northeast Fisheries Science Center, Milford, CT

Received 12 May 2022, accepted 14 August 2022, DOI: 10.1111/php.13693

ABSTRACT

Nonphotochemical quenching (NPQ) is known to depress *in vivo* fluorescence (IVF) of chlorophyll *a* (Chl*a*) in aquatic environments, which makes it difficult to interpret the hour-to-hour variations in Chl*a* measured by *in situ* fluorometers. We hypothesized that ratios between quenched and unquenched IVF are a function of both NPQ and photochemical quenching. In this study, two diatom model species *Thalassiosira pseudonana* (CCMP1335) and *Thalassiosira weissflogii* (CCMP1047) incubated under a sinusoidal light:dark cycle were studied; IVF was recorded continuously, and Chl*a* and photophysiological variables were measured seven times a day. The maximal decline in Chl*a*-specific IVF (IVF^B) attributable to quenching was 50% under the experimental settings. An NPQ and photochemical quenching-based modeling equation exhibited a better match to the measured IVF^B than equations representing the sole NPQ effect. Photochemical quenching induced by measuring light beam varied substantially during the day, and the part of the model for this process is excitation intensity-dependent (which is differed between models of *in situ* fluorometers, implying no straightforward method to correct Chl*a* for all instrument models, instrument-specific parameterization is required). The forms of the IVF^B-light relationship are discussed as well. The findings foster a holistic understanding of NPQ effects on *in vivo* Chl*a* fluorometry.

INTRODUCTION

In vivo fluorometry of chlorophyll *a* has been used widely in aquatic environments for continuous monitoring of spatiotemporal changes in phytoplankton biomass (1). The use of *in vivo* fluorometry has facilitated observations and comparisons of chlorophyll *a* (Chl*a*) in the sea at various time intervals (*e.g.* daily, weekly, and interannually) in a cost-effective way (2,3). Reliability of hourly measurements, however, remains problematic (4-7). Although Chl*a* concentration is estimated by this method, it is *in vivo* fluorescence (IVF) that is actually measured. IVF is the light re-emitted by photosystems from excited to ground states. Chl*a*-specific IVF (IVF^B) is variable and can be affected by phytoplankton taxonomy (8,9), cell size (10), nonphotochemical quenching (4,7,11,12,13), temperature (1,14) and nutrient status (15). Nonphotochemical quenching (NPQ) is a protection mechanism used by plants and algae to dissipate excess absorbed light energy as heat (*i.e.* photochemistry + fluorescence emission + heat dissipation = absorbed light energy); consequently, quantum yield of fluorescence (the ratio between fluorescence emitted and photons absorbed) is reduced as the dissipation rate increases (16). Sunlight intensity changes constantly during the day, and NPQ is extremely sensitive to light intensity (17,18). Accordingly, on an hourly basis, NPQ effects upon IVF^B are dynamic. In coastal waters, where diatoms often dominate (19), hydrographic dynamics, such as tidal advection and wind-induced turbulence, also contribute to the hour-to-hour variation in actual Chl*a* (20,21). The IVF variabilities driven by NPQ and Chl*a* are blended. As a result, correcting NPQ effects becomes one of the biggest challenges for *in vivo* fluorometry. Nevertheless, *in vivo* fluorometry is the favored method for monitoring phytoplankton biomass in coastal waters because other methods that are not IVF-based (such as the particulate backscattering method and the absorption line height method) have severe issues attributable to turbidity and biofouling (22,23).

To correct for NPQ effects, indirect methods assumed that Chl*a* was homogenous within the mixed layer and at a steady state between growth and loss, and then, the unquenched IVF at deep layers or during the night was taken for extrapolation (4,11), thereby removing quenched IVF. Recently, a machine-learning method to perform the direct correction was reported (7). We believe that a straightforward, mathematical correction has practical potential. Such a correction can help to monitor rapid changes in Chl*a* arising from short-lived algal blooms (24), patchiness (25) or consumption by suspension feeders (6,26). However, a limited understanding of NPQ effects on IVF^B has been a bottleneck restricting direct correction. For instance, the role of photochemical quenching in the determination of IVF^B regarding NPQ remains unclear, and forms of the IVF^B-light relationship (exponential or sigmoid) are also underexplored. In this report, NPQ and IVF^B of diatoms were measured simultaneously under environmentally relevant nutrient concentrations and light condition, revealing subtle mechanisms and updated quantitative relationships between NPQ and IVF^B to highlight the level of confidence one should expect from environmental *in vivo* fluorescence data.

*Corresponding author email: xieyuyuan@hotmail.com (Yuyuan Xie)
†Current address: College of Marine Science, University of South Florida

MATERIALS AND METHODS

Mechanistic equations. The general equation for IVF (27) is

$$\mathrm{IVF} = I_{\mathrm{ex}} \quad a_{\mathrm{LHII}} \quad \phi_{\mathrm{F}} \quad Q_a \quad G \tag{1}$$

In the equation, I_{ex} is the intensity of excitation light beam, a_{LHII} is the absorption coefficient of photosystem II (PSII) light-harvesting apparatus, ϕ_F is the quantum yield of fluorescence, Q_a quantifies reduced fluorescence due to the package effect, and G is the instrument-specific detection efficiency. The term qP is photochemical quenching (the process in which ϕ_F is reduced with increased photochemical reaction rates) and has been taken as an estimate of the fraction of open PSII reaction centers (28); the use of $(1 \quad qP)$ can derive ϕ_F from minimum and maximum quantum yields of fluorescence (ϕ_{F0} and $\phi_{F\mathrm{m}}$) (29).

$$\phi_F = \phi_{F0} + (\phi_{F\mathrm{m}} \quad \phi_{F0})(1 \quad qP) \tag{2a}$$

Furthermore, the Poisson possibility of a PSII reaction center remaining in the open state is a natural exponential function of the ambient light (I) (30).

$$\phi_F = \phi_{F0} + (\phi_{F\mathrm{m}} \quad \phi_{F0}) \quad 1 \quad e^{(\quad \alpha I)} \tag{2b}$$

In the equation, α is the initial slope for the proportion of closed PSII reaction centers against I. Because the I_{ex} of an *in situ* Chl*a* fluorometer is constant, and it is reasonable to consider the variations of a_{LHII}, Q_a, and G are neglectable for studies of single phytoplankton culture, Eq. 2b can be replaced by

$$F(I_{ex}) = F_0 + (F_{\mathrm{m}} \quad F_0) \quad 1 \quad e^{(\quad \alpha I_{\mathrm{ex}})} \tag{3a}$$

Under the light-regulated state, F_0 and F_{m} become F'_0 and F'_{m} because of NPQ, then

$$F(I_{\mathrm{ex}}) = F'_0 + \quad F'_{\mathrm{m}} \quad F'_0 \quad 1 \quad e^{(\quad \alpha I_{\mathrm{ex}})} \tag{3b}$$

Accordingly, the IVF detected by an *in situ* Chl*a* fluorometer could be simulated by using an active fluorescence technique, for example, fast repetition rate fluorometry or a fluorescence induction and relaxation technique (31,32). Conceptually, there are three modes of *in vivo* fluorometry related to I_{ex}: F_0−, F_{m}−, and F−modes (33). I_{ex} of F_0−mode must be small enough to not induce closure of PSII reaction centers. F_{m}−mode demands a short (100 µs), saturating light pulse to induce F_{m} (31,33). I_{ex} of F−mode is somewhere between. *In situ* Chl*a* fluorometers usually operate in the F−mode for balancing all factors (such as manufacturing, signal strength, and accuracy). Based upon the Eq. 3b, $F(I_{\mathrm{ex}})$ would be at the same position between F'_0 and F'_{m} if α is constant throughout the day, through which photochemical quenching does not contribute to the variation in IVF; however, results of previous research that studied on the diel variation of phytoplankton photo-physiology implied that α is indeed varying with the ambient light condition (34,35). We proposed that photochemical quenching plays an important role in the determination of IVF. The extent of the variation in α and the impacts of varying α on the diurnal pattern of IVF were studied to confirm this hypothesis.

Morrison (29) has proposed an empirical equation to model sunlight-induced Chl*a* fluorescence during the daytime. That equation can model the smooth responses of IVF to changing light intensity. That equation was modified to fit for our work.

$$F(I_{\mathrm{ex}}) = \left[r + (1 \quad r)e^{\quad I/I_{\mathrm{T}}}\right]\left[F_0 + (F_{\mathrm{m}} \quad F_0) \quad 1 \quad e^{(\quad \alpha I_{\mathrm{ex}})}\right] \tag{4a}$$

where r scaled between 0 and 1 is the constant fraction of photosystem II that is unaffected by NPQ by assumption, $(1 \quad r)$ might represent the maximum quenching by NPQ, I_{T} is the light constant at which NPQ reaches the half of its maximal capacity. Serodio and Lavaud (36) parameterized the function of light for NPQ following the Hill equation, which depicts the protein-ligand binding kinetics for activation of cofactors and quenchers of energy-dependent NPQ (16). The equation shows that NPQ cannot increase infinitely with light, namely there is a maximum, and the ratio between the discrete and maximal NPQ is a sigmoid function of light (36,37). Thus, we defined the sigmoid alternative of the Eq. 4a as follows

$$F(I_{\mathrm{ex}}) = \quad r + (1 \quad r)\frac{I_{50}^n}{I_{50}^n + I^n}\left[F_0 + (F_{\mathrm{m}} \quad F_0) \quad 1 \quad e^{(\quad \alpha I_{\mathrm{ex}})}\right] \tag{4b}$$

where n is the Hill coefficient and I_{50} is the constant of half saturation light. The average value of n for diatoms is 1.60 (36), which was used in this study.

Chla probes. Four Chl*a* probes were used in this study, and each was composed of a cyclops-7 Chl*a* sensor (Turner Designs) and a data logger (Precision Measurement Engineering). The I_{ex} was approximately 80 µmol photons m^{-2} s^{-1} measured by using an LI-192 quantum sensor (LI-COR Biosciences) at the focal point. The Chl*a* probes were calibrated with rhodamine (Turner Designs) and cross-calibrated following the procedure of Cremella *et al.* (38). The measuring frequency was set as one value per minute. Data logger clocks were synchronized before each experiment. Probe shells were cleaned and sterilized with ethanol.

Batch culture, sampling, and basic measurements. *Thalassiosira pseudonana* (CCMP1335) and *Thalassiosira weissflogii* (CCMP1047) isolated from Long Island Sound were cultured for experiments. Diatoms were inoculated under dim light at the beginning then transferred to the experimental light (and temperature) condition for acclimation. Light was provided by a cool-white LED panel (superbrightleds.com). A programmed controller was used for simulating the sinusoidal light: dark (12:12) cycle, with the highest of 600 µmol photons m^{-2} s^{-1} (Figure S1) at noon. For the experimental settings to have the environmental and ecophysiological relevant magnitude of the light intensities and their diel variations in the coastal waters, the highest light intensity was the estimated mean midday photosynthetically available radiation (PAR) of the mixed layer between April and September in the Long Island Sound, a temperate estuary in the Atlantic coast of USA (details on the estimate can be found in Appendix S2; Figure S2). The months from October to March were not included in the estimate because there was insufficient light to generate appreciable NPQ.

After at least eight generations, the acclimated culture in the exponential phase of growth was transferred again to four cylinder-shaped borosilicate glass bottles (KIMAX, Kimble), each filled with 8 L f/40 medium and labeled with letters (A, B, C, and D). The amounts of nutrients were based upon calculations to ensure that: (1) diatoms would grow without nutrient limitation starting from an established cell density, and (2) the amount was within the range of coastal environments. The sterilized Chl*a* probes were placed inside the bottles. Magnetic stir bars were used to create vortex flow inside the bottles for two purposes: (1) to allow the phytoplankton cells to experience the same light condition and (2) to induce water flow in and out of the probe chamber for a homogeneous exposure of probe to phytoplankton cells. Light intensity was recorded continuously at the average distance of the bottles from the LED panel by using the LI-192 quantum sensor and a LI-1500 logger (LI-COR Biosciences).

Sampling was conducted for 2 days (during exponential growth) before the population became too dense, and nutrients were exhausted, at which point, photo-physiological status would be greatly changed. Sampling was performed seven times a day at 5:00 (before turning on the light), 7:00, 9:30, 12:00, 14:30, 17:00 and 19:00 (after turning off the light). Water samples were collected from bottle bottom taps. Immediately after tap sampling, an aliquot of 4 mL fresh sample was transferred to a glass cuvette for the photo-physiological measurement, and the rest was stored in the dark in an icebox for filtration. Aliquots of 30 mL were filtered onto 25-mm diameter GF/F glass fiber filters (Whatman) for Chl*a* analysis and temporarily stored in glass tubes in a −20°C freezer (immediately analyzed after incubation). Aliquots of 2 mL were mixed with 4% (v/v) formalin for cell counts. In addition, nutrient samples were collected at the beginning and the end and stored at −20°C before analysis. See Appendix S3 for analytical methods of Chl*a*, cell density and nutrients. Growth rate (µ) was computed by

$$\mu = \frac{\ln B_2 \quad \ln B_1}{t_2 \quad t_1} \tag{5a}$$

$$\mu = \frac{\ln b_2 \quad \ln b_1}{t_2 \quad t_1} \tag{5b}$$

where B and b were Chl*a* concentration and cell density, respectively, and t was time (h).

Processing of IVF data. When incubation ended, the IVF data were downloaded from the probes and archived on a secure network server. Then, quality control, including time format conversion, temperature correction, removing apparent outliers, and cross-calibration, was performed on the data (see Appendix S4). To estimate IVF^B, Chl*a* at each time point was estimated from the exponential function $[\ln B_2 = \ln B_1 + \mu(t_2 \quad t_1)]$ for simplicity, although this process would overlook circadian variations. Then, IVF^B was computed by normalizing IVF to Chl*a*. To remove any IVF^B trends caused by factors other than NPQ, a straight line was drawn through the 6:00 and 18:00 points and used as the unquenched IVF^B. Finally, the quenching ratio Q% was calculated.

$$Q\% = \frac{IVF_{quenched} \quad IVF_{unquenched}}{IVF_{unquenched}} \tag{6}$$

Photo-physiological analysis and calculation of photo-physiological variables. The sample in the glass cuvette was placed in a fluorescence induction and relaxation (FIRe) system (Satlantic, Canada) for photo-physiological analysis. The method of single turnover active fluorometry (31) was used. The measuring protocol is displayed in Figure S3 and detailed in Appendix S5. F' and F'_m for incubation light intensity and a series of actinic light were measured. $F'_{0(2s)}$ and $F'_{m(2s)}$ were also measured with 2-s dark period that is required to allow reopening of closed PSII reaction centers (39). The $F'_{0(2s)}$ and $F'_{m(2s)}$ at dawn (those with the highest $F'_v/F'_{m(2s)}$) was taken as the dark-acclimated (in other words, NPQ not present) values $F_{0(t0)}$ and $F_{m(t0)}$. These values were critical as the baseline for calculation of the Stern-Volmer parameter $NPQ_{SV(t)}$ (40).

$$NPQ_{SV(t)} = \frac{F_{m(t0)}}{F'_m} \quad 1 \tag{7}$$

The light-regulated maximum quantum yield of PSII was expressed as

$$F'_v/F'_{m(2s)} = \quad F'_{m(2s)} \quad F'_{0(2s)} \quad /F'_{m(2s)}. \tag{8}$$

Fast and slow components of NPQ and the normalized Stern-Volmer coefficient (NPQ_{NSV}) were also calculated for complementary results (see Appendix S6), a higher NPQ_{NSV} value means more energy will be dissipated (41). The minimum fluorescence associated with F'_m was calculated by

$$F'_{0,calc} = F'_{0(2s)} \quad 1 \quad \frac{F'_{0(2s)}}{F'_{m(2s)}} + \frac{F'_{0(2s)}}{F'_m} \Bigg) \Bigg(\quad ^1 \tag{9}$$

Then, photochemical quenching (qP) was computed by

$$qP = \frac{F'_m \quad F'}{F'_m \quad F'_{0,calc}} \tag{10}$$

The partial derivative of α was

$$\alpha = \frac{\partial(1 \quad qP)}{\partial I}_{qP=1} \tag{11}$$

To allow for direct comparison, the volumetric values ($F'_{0,calc}$ and F'_m) were firstly corrected for different gain settings and secondly normalized to Chl*a* to get $F'^B_{0,calc}$ and F'^B_m. With the known photo-physiological parameters, $F(I_{ex})$ and normalized $F(I_{ex})$ $[F^B(I_{ex})]$ can be computed, respectively, by

$$F(I_{ex}) = F'_{0,calc} + \quad F'_m \quad F'_{0,calc} \quad 1 \quad e^{(\quad \alpha I_{ex})} \tag{12a}$$

$$F^B(I_{ex}) = F'^B_{0,calc} + \quad F'^B_m \quad F'^B_{0,calc} \quad 1 \quad e^{(\quad \alpha I_{ex})} \tag{12b}$$

The smaller diatom *T. pseudonana* showed an unusual fluorescence induction trace on the second sampling day (Figure S4). The induction trace, however, returned to normal by the excitation of the combination of blue and green light. This phenomenon might be attributed to triplet quenching and triplet-triplet transfer (see Appendix S7). Although a special program was performed to obtain the photo-physiological variables (see Appendix S7), those data were excluded for comparison.

Model experiments. To obtain model coefficients of Eq. 4a and 4b, optimization with the "optim" function of the "stats" package of the R software was performed. Furthermore, to simulate varying α, an analytical subroutine to derive α was embedded in the optimization (see Appendix S8, fluorescence-chlorophyll inversion for diurnal cycle (ConFID) model), model coefficients were compared between constant and varying α. The models were assessed by both root-mean-square error (RMSE) and visual inspection for normality of residuals. In addition to the laboratory data, data measured *in situ* in Harpswell Sound, Maine, USA (4) were also analyzed. The values digitized from the published figures were used.

RESULTS AND DISCUSSION

Chl*a* concentration, cell density and nutrients

Both *T. weissflogii* and *T. pseudonana* grew exponentially during the sampling periods (Fig. 1). The Chl*a*-based μ of *T. weissflogii* and *T. pseudonana* were 0.079 0.010 h^{-1} and 0.053 0.002 h^{-1}, respectively; the density-based μ were 0.102 0.007 h^{-1} and 0.065 0.002 h^{-1}, respectively (Table 1). Higher cell-density-based μ than Chl*a*-based μ was observed, reflecting the phenomenon that diatoms decrease in size and Chl*a* per cell with each cell division. At the end of sampling, *T. weissflogii* reached the Chl*a* concentration of 23.7 8.2 μg L^{-1} and cell density of (16 4) × 10^3 cells mL^{-1}, whereas *T. pseudonana* reached a mean Chl*a* concentration of 101.8 7.4 μg L^{-1} and cell density of (393 8) × 10^3 cells mL^{-1}. Nutrient concentrations at the end of the sampling were greater than half of what initially was added in the media (Table S2), indicating that growth did not become nutrient-limited.

Time series of IVF^B

The time series of IVF in the two days exhibited two distinctive features: an overall exponential increase of IVF and periods of depressed values during the daytime that formed two "U" shapes embedded in the increasing trend (Fig. 1C,G). The two "U" shapes during the daytime could be seen clearly by normalizing the IVF to the Chl*a* (namely IVF^B) (Fig. 1D,H). Ranges of IVF^B were similar between the two species. *T. pseudonana* demonstrated a decreasing trend of IVF^B on the second day attributable to triplet quenching (see Appendix S7 and Figure S4), but *T. weissflogii* did not.

Relating diurnal variations in IVF^B to NPQ and photochemical quenching

F'^B_m underwent diurnal cycles (Fig. 2A,E) with higher values at 5:00, 7:00, 17:00, 19:00 and lower values between 9:30 and 14:30. The absolute magnitudes of F'^B_m on both days were similar for *T. weissflogii* (Fig. 2A), but lower on the second day for *T. pseudonana* (Fig. 2E). The $NPQ_{SV(t)}$ of both *T. pseudonana* and *T. weissflogii* was generally lower than 0.2 at 5:00, 7:00, 17:00, 19:00 and around 1.1 between 9:30 and 14:30 (Fig. 2B,F) except the $NPQ_{SV(t)}$ of *T. pseudonana* was 1.8–1.9 at 12:00 and 14:30 on the second day (Fig. 2F). The analysis of NPQ components showed that NPQ relaxed quickly during the first 2 s while generally 40% of total $NPQ_{SV(t)}$ remained at 30 s reflecting a slow process of NPQ recovery (Figure S5). The $F'_v/F'_{m(2s)}$ of *T. weissflogii* was about 0.56 at 5:00 and 7:00, then decreased gradually

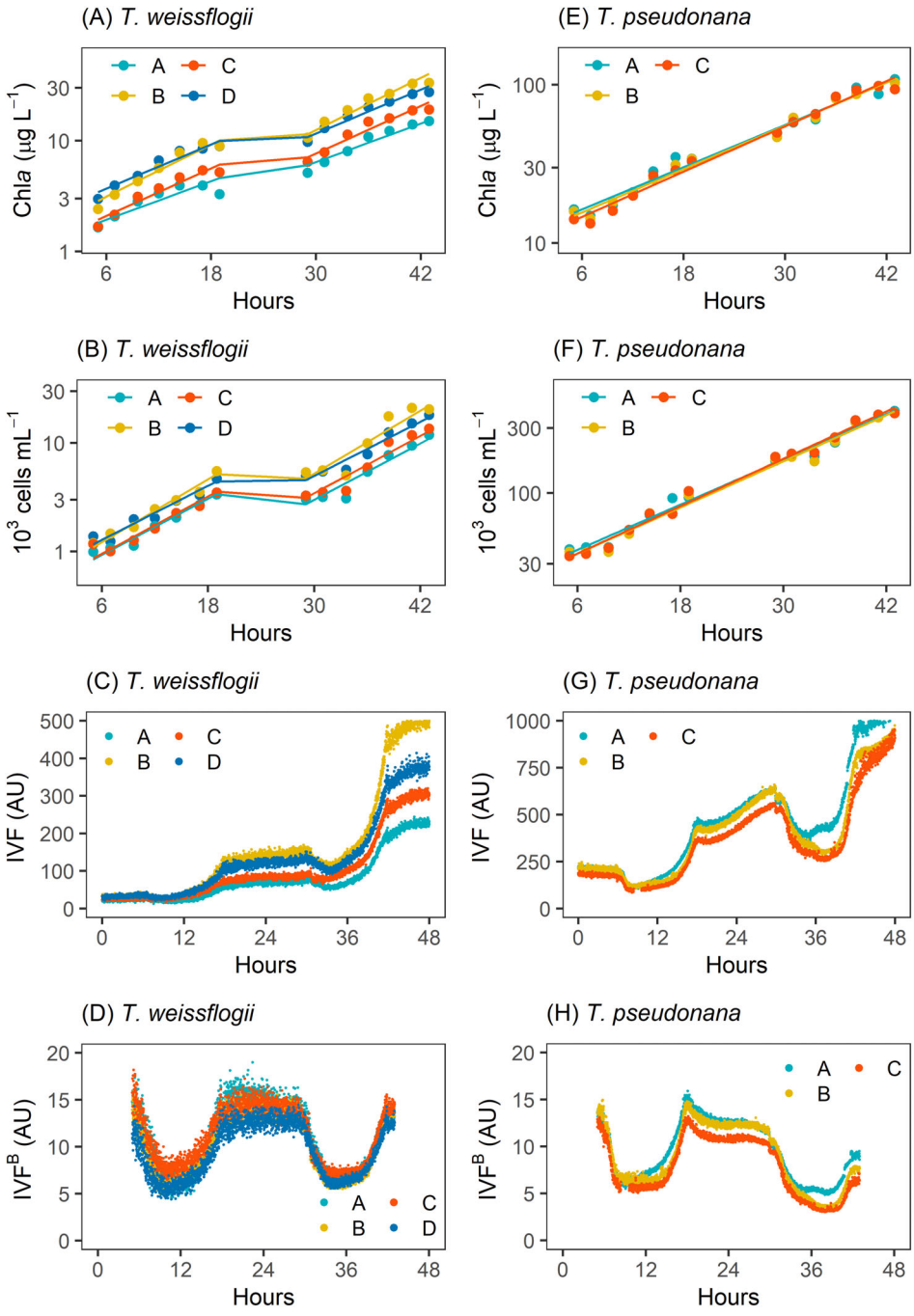

Figure 1. Exponential increases in (A, E) Chl*a* concentration, (B, F) cell density and (C, G) *in vivo* fluorescence (IVF) of *T. weissflogii* and *T. pseudonana* over time. (D, H) Chl*a*-specific IVF (IVF^B). 12 AM of the first sampling day was set as the hour zero. Replicates are displayed in different colors and labeled with letters.

to 0.33 at 14:30 until recovering during dusk and dark (Figure S6). A similar pattern was observed for *T. pseudonana* on the second day, but a different pattern than on the first day (higher $F'_v/F'_{m(2s)}$ in the dusk than in the dawn) might reflect an acclimation process (Figure S6). The NPQ_{NSV} of *T. weissflogii* was 0.80 in the dark, then increasing after 7:00, reaching a peak of 2.00 at 14:30 (Figure S6). The increased NPQ_{NSV} indicated additional quenching which was dynamic during the day; a similar pattern for *T. pseudonana* was observed on the second day (Figure S6).

There were three general features in the relationship between (1 *qP*) and actinic light, as well as time (Fig. 2C,G). Firstly, (1 *qP*) *versus* actinic light was characterized as an exponential saturation curve. Secondly, the curve displayed the steepest slope in the dark, and a much gentler slope between 9:30 and 14:30, with a transition at 7:00 or 17:00; the resulting α showed significant diurnal variations, with much higher α at 5:00 and 19:00 (Fig. 2D,H). Lastly, the curve's saturation point varied with time, day and species. It was intriguing that the saturation points were substantially lower than 1. After a literature review, we found

Table 1. Mean growth rates (μ) calculated from Chl*a* concentration and cell density of *T. weissflogii* and *T. pseudonana*. The $P > 0.05$ indicated that μ was not different between replicates as tested by analysis of covariance on the slopes of linear regressions shown in Fig. 1

		Chl*a*			Cells		
Species	*N*	μ (h^{-1})		*P*	μ (h^{-1})		*P*
T. weissflogii	4	0.079	0.010	0.016	0.102	0.007	0.24
T. pseudonana	3	0.053	0.002	0.72	0.065	0.002	0.74

that $1 - e^{(-\alpha I)}$ is not the most appropriate expression of $(1 - qP)$, and the mechanical expression of qP is based upon the Poisson possibility by which qP is the ratio between occurrence of PSII charge separation and multiple hits of photons on the functional cross section of PSII (σ) over the time scale τ (the unit time for PSII to process one PSII charge separation) (42).

$$qP = \frac{1 - e^{(-\sigma\tau I)}}{\sigma\tau I} \tag{13}$$

This equation explained the varied saturation points. Eq. 13 yielded better converge on $\sigma\tau$ than $1 - e^{(-\alpha I)}$ on α; thus, $\sigma\tau$

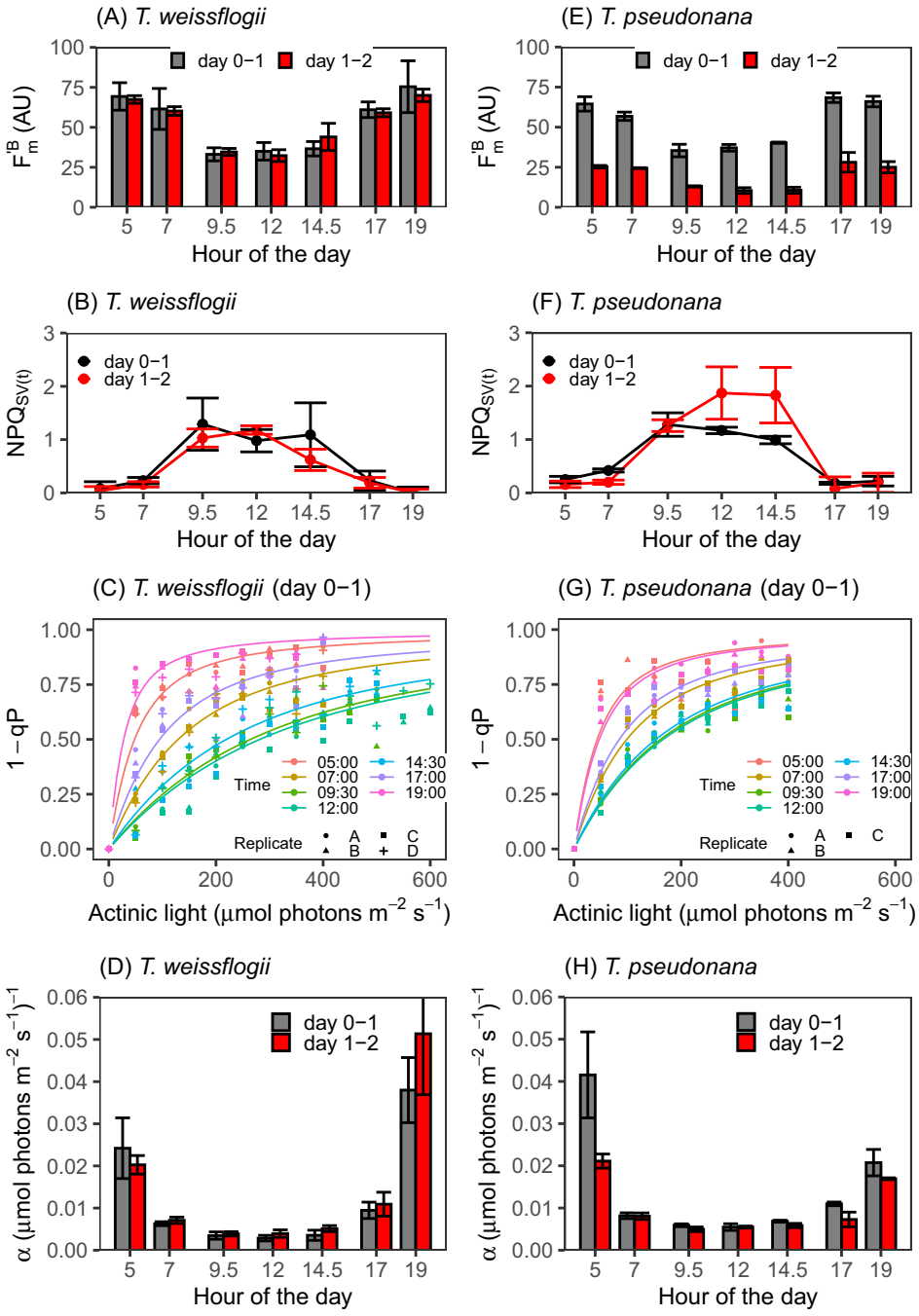

Figure 2. Diurnal variations in averages standard deviations of (A, E) F'_m, (B, F) $NPQ_{SV(t)}$ and (D, H) α of *T. weissflogii* and *T. pseudonana*. (C, G) relationships between $1 - qP$ and actinic light as well as time for day 0–1, same subplots in Figure S6 for day 1–2.

was taken as α. NPQ was one of the underlying mechanisms of varying α. A recent study in another diatom model species, *Phaeodactylum tricornutum*, reported a precise negative correlation between NPQ and σ (43), which suggests the higher the NPQ, the lower the proportion of PSII reaction centers being in the closed state (because of the lower possibility of the absorbed photon to be used for photochemistry) for a given intensity of illumination, thereby reducing excitation pressure and the risk of photoinhibition (44). Consequently, α is lower with higher NPQ. This mechanism has been also verified for green algae but not for picocyanobacteria (35).

The influences of varying α on IVF^B are illustrated in Fig. 3; IVF^B in the dark was close to F'^B_m and distant from F'^B_0; when light was turned on and the light intensity was increased constantly, F'^B_m decreased quickly because of increasing $NPQ_{SV(t)}$, but IVF^B decreased more as a consequence of decreasing α (Fig. 2); this shift resulted in IVF^B near midday (approximately between 9:30 and 14:30) being close to F'^B_0 and distant from F'^B_m. Thereafter, IVF^B recovered in the late afternoon and returned to the dark value, which was close to F'^B_m. The linear regression between IVF^B and F'^B_0 displayed a small coefficient of determination (R^2) ($R^2 = 0.56$) indicating that IVF^B did not follow F'^B_0 (Fig. 4A). The R^2 was 0.84 for F'^B_m (Fig. 4B) and 0.88 for $F^B(I_{ex})$ showing the variation of IVF^B was most consistent with that of $F^B(I_{ex})$ (Fig. 4C). The α value in the dark was about 0.020 (µmol photons m^{-2} $s^{-1})^{-1}$, then $1 - e^{(-\alpha I_{ex})} = 0.80$ which made the IVF^B in the dark approach F'^B_m and account for the better correlation of IVF^B with $F^B(I_{ex})$ and F'^B_m than with F'^B_0. But if α was an incorrectly assumed constant, IVF^B would be at the same position between F'^B_m and F'^B_0 over the time. Similarly, the linear regression between IVF and $F(I_{ex})$ showed the highest R^2 (Fig. 4F). To summarize, NPQ has been shown to be the major factor accounting for the diurnal IVF^B reductions, but the contribution of photochemical quenching cannot be neglected. Based on the above understanding, optimization was performed to obtain coefficients of compensating models. Optimized r values were 0.348 and 0.334, respectively, for Eq. 4a and 4b. The derived I_T of Eq. 4a was approximately 400 µmol photons m^{-2} s^{-1}, while the I_{50} of Eq. 4b was about 288 µmol photons m^{-2} s^{-1} (Fig. 5). These NPQ-based equations fit fairly well with this study's data, yielding RMSE of 0.054 and 0.051, respectively.

Sigmoid light function for NPQ

The difference between Eq. 4a and 4b depicted in the graphics was that Eq. 4a estimated greater quenching when I was below 200 µmol photons m^{-2} s^{-1} (Fig. 5), although the difference was too small to determine which model was better. Nonetheless, model optimization was also performed on the published environmental data. The optimization showed similar results, Eq. 4a overestimated quenching when I was <500 µmol photons m^{-2} s^{-1}; by contrast, Eq. 4b slightly improved the modeled quenching under low light conditions (Fig. 5), and the optimized r and I_{50} were 0.140 and 900 µmol photons m^{-2} s^{-1}, respectively. More importantly, the use of Eq. 4b improved reliability of model optimization. The idea of a sigmoid light function for NPQ is supported by literature (16,36). The sigmoid shape is determined by cooperativity in enzyme kinetics, reflecting increased affinity for cofactors or quenchers with development of NPQ. However, Lepetit *et al.* (37) found distinct responses of NPQ to fluctuating and steady sinusoidal light cycle, respectively, and different types of responses were regulated by different sets of genes. The intense NPQ responses to fluctuating sinusoidal light cycle would lead to a responsive curve similar to Eq. 4a (40). Thus, model coefficients reflected different degrees of mixing between this study and the Harpswell sound environment. Alternatively, the shape of the light function for NPQ could also be affected by the residence time of water in the measuring chamber. At 7:00 and 17:00 when $NPQ_{SV(t)}$ was low, NPQ could be largely relieved at 2 s (Fig. 5 and Figure S5) for a long residence time making the IVF^B curve flatter during those time ranges; thus, a sigmoid curve would match. Studies revealed that diatom NPQ consists of different components with different kinetics, and occurrence of all components is not simultaneous but rather additive based upon light conditions (37,43). The fastest component usually comes first, while high light conditions tend to induce sustained components of NPQ which require longer time to relieve (Figure S5).

Influences of varying α upon IVF^B

With the subroutine to derive varying α, the ConFID model reproduced the same curve (Fig. 3) as that depicted by Eq. 4b (Fig. 5), but model coefficients were different. The tight coupling

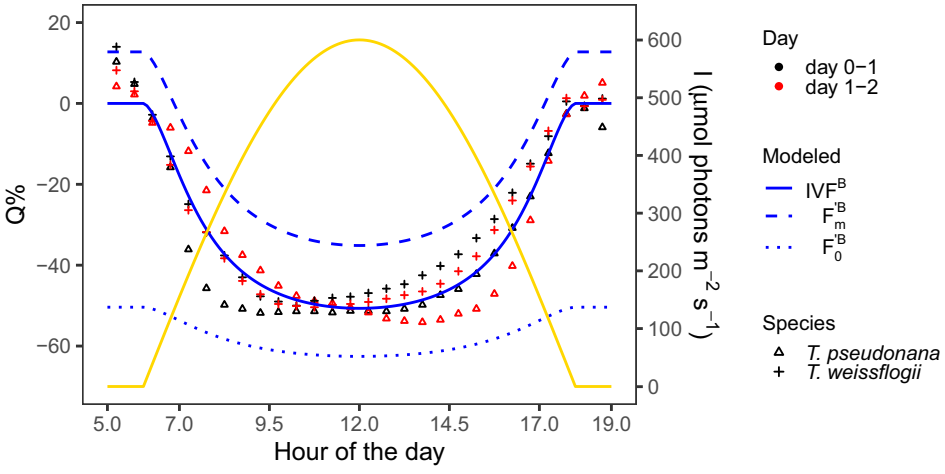

Figure 3. Comparison between the measured and modeled percentage of quenching (Q%). Yellow line represented the incubation light intensities.

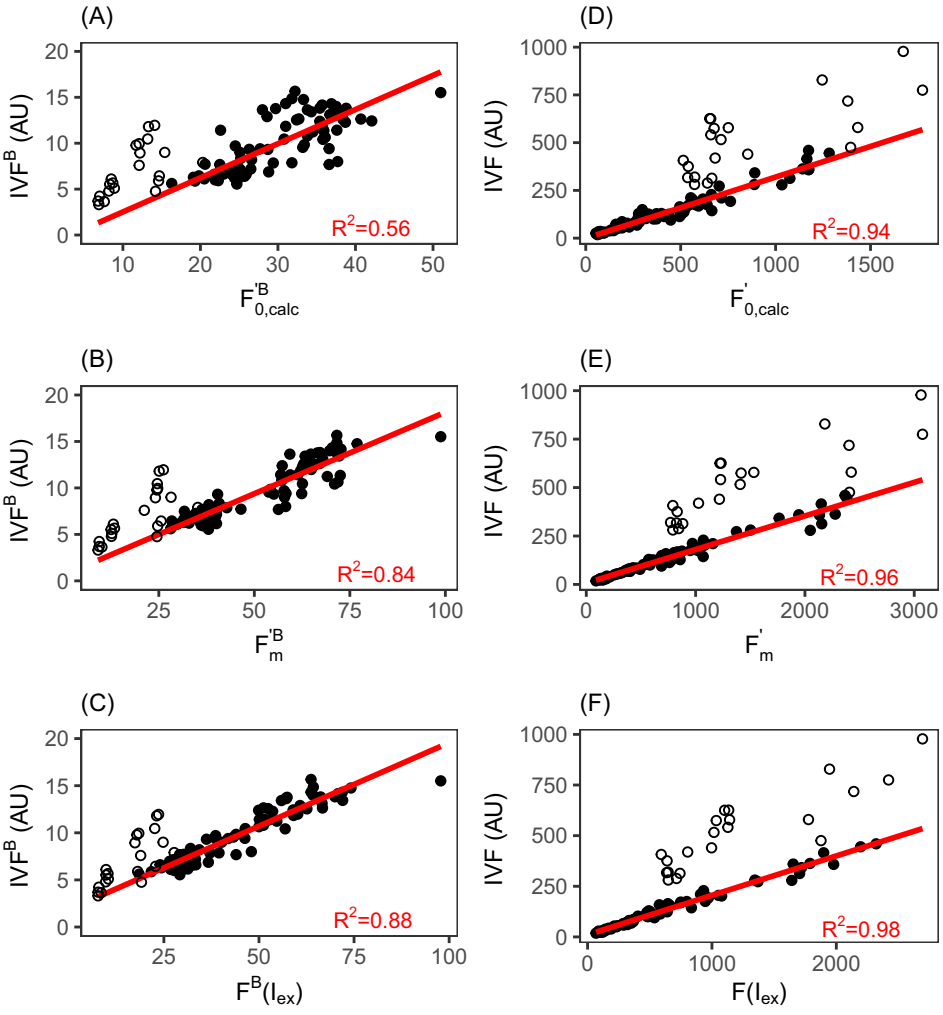

Figure 4. Comparisons between IVF^B and (A) $F'^B_{0,calc}$, (B) F'^B_m, (C) the calculated $F^B(I_{ex})$. Similar comparisons for (D–F) the volumetric values. The red lines were model II linear regressions. *T. pseudonana* on day 1–2 (open dots) were excluded for analysis because of influences of triplet quenching.

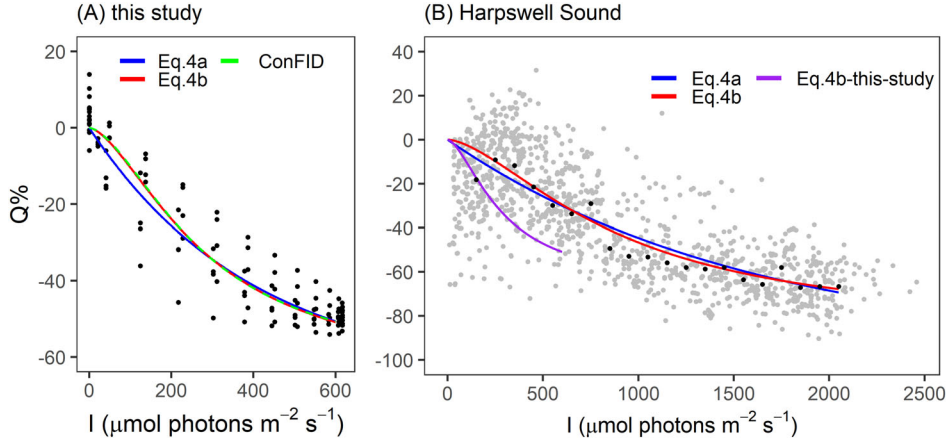

Figure 5. Comparisons of different models for (A) experimental data of this study and (B) field data in the Harpswell Sound, Maine, USA (extracted from Ref. 4). Black dots in (B) are medians.

between NPQ and α indicates that I_{50} and n optimized by the ConFID model can be used only for reference, if without validation, because the coefficients are dependent upon how α is modeled. Here, the measured α was used for validation (Figure S7). Finally, the optimized I_{50} was 320 μmol photons m^{-2} s^{-1}, and a lower maximum NPQ was found (indicated by

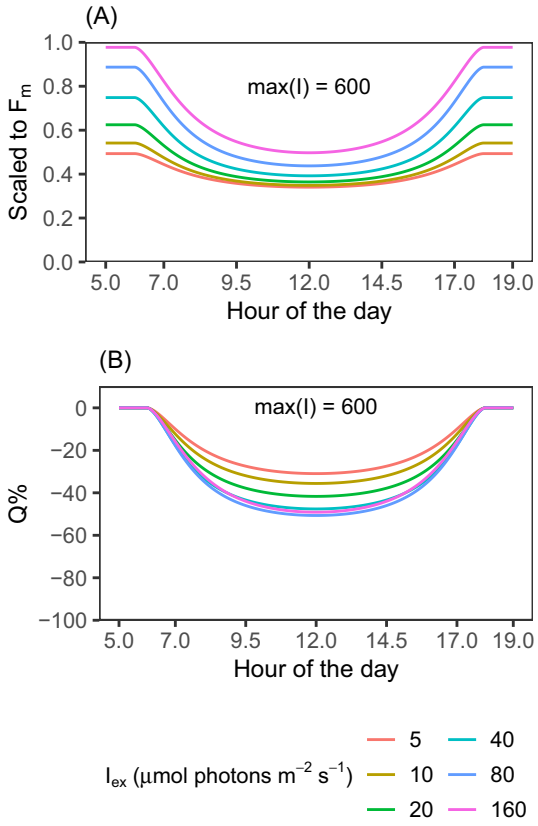

Figure 6. Influences of different I_{ex} on NPQ effects on *in vivo* fluorometry of Chl*a* displayed as both (A) magnitude scaled to F_m and (B) percentage of quenching (Q%) against time.

$r = 0.420$ comparing to 0.334 by Eq. 4b). Consequently, the clarification of the relationship between IVF^B and F'^B_m, as well as F'^B_0, is important for the research effort to recover NPQ_{SV} information from the diurnal variation in IVF^B (45).

We also analyzed the potential impacts of varying α on the use of *in situ* Chl*a* fluorometers with different I_{ex}. Output of the ConFID model with a possible range of I_{ex} for commonly used *in situ* Chl*a* fluorometers (5, 10, 20, 40, 80 and 160 µmol photons m^{-2} s^{-1}, the lowest number was determined according to the configuration provided by Beutler *et al.* (46), and the highest number was simply the double of I_{ex} used in this study) was computed. Both Q% and absolute values of IVF^B were evaluated. Firstly, IVF^B declined proportionally to I_{ex} (data not shown). Secondly, decreased I_{ex} made the IVF^B curve gentler to some extent but did not eliminate the depression (Fig. 6); low absolute values of IVF^B caused by a small I_{ex} will also sacrifice detection limit and signal-to-noise ratio, thereby prohibiting use of *in situ* Chl*a* fluorometers in some waters with low phytoplankton biomass or at times when biomass is low. Thirdly, results showed a large difference in IVF^B in the dark (scaled to the dark-acclimated F_m) because of substantial divergence in photochemical quenching, without NPQ present, the large fraction of absorbed photons is used for photochemistry; then, reaction centers will be oxidized/closed quickly with the increased intensity of excitation light; thus, IVF^B will change greatly as a function of I_{ex}, By contrast, with NPQ present during midday, F'^B_0 and F'^B_m are depressed, and then, variable fluorescence is smaller, and a smaller fraction of absorbed photons used for photochemistry leads to less photochemical quenching. IVF^B, therefore, will show a small variation for different I_{ex} during midday (Fig. 6A). If we adapted Eq. 4a and 4b to different models and/or brands of *in situ* Chl*a* fluorometers (simulated by different I_{ex}) that are pre-calibrated in the dark, the equations would significantly overestimate the quenching during midday for a small I_{ex} (Fig. 6B; and Fig. 4 in Rousso *et al.* (12)), subsequently overestimate Chl*a* by correction for NPQ effects. The implication is that an NPQ correction for IVF^B could be fluorometer specific.

Limitations of this study

PSII photoinactivation is the process of light-induced damage to PSII and can be reversed by repair reactions (47). The maximum light intensity used in this study was 600 µmol m^{-2} s^{-1}, which was much higher than the half-saturation light for growth (48,49). Thus, net PSII photoinactivation could occur when instantaneous light intensity was above a threshold, although the overall effect of photoinactivation upon growth rate might be small. Increased $F'_{0(2s)}$ is one of the consequences of net PSII photoinactivation (47), and IVF^B would be increased accordingly. The existence and extent of photoinactivation could not be assessed without the knowledge of F_0 and F_m, which were difficult to measure under the light-regulated state (47). Thus, for simplicity, the models in this study did not take photoinactivation into account. The limitation may account for the overestimated quenching in the afternoon (Fig. 3), leading to the asymmetrical pattern (12).

Insufficient dark acclimation is another reason accounting for the difficulty in obtaining true F_0 and F_m. Energy-dependent quenching (qE) contributes most NPQ for diatoms. It is known that qE of diatoms requires activation of both light-harvesting complex stress-related (LHCX) proteins and the xanthophyll cycle pigment diatoxanthin (43,50). In addition, a pH gradient is required for activation of diatoxanthin as the quencher (51) but not for maintaining this quenching (18). If diatoxanthin is already activated, absence of a pH gradient cannot completely relieve qE; instead, there will be two relaxing stages (Figure S5) comprised of a sharp drop within seconds (the mechanism is unclear) and a slow process that is diatoxanthin-dependent. A certain level of light illumination is essential for diatoms to generate NADPH to perform the epoxidation of diatoxanthin; therefore, qE can be fully relaxed (18). But for logistical reasons, dark acclimation was not conducted at measurements between 7:00 and 17:00; then, uncertainty in calculating the NPQ parameter was introduced. However, it is reasonable to assume F_m to be constant throughout the day (40); thus, it is appropriate to use the $NPQ_{SV(t)}$ calculated by taking the $F_{m(t0)}$ as the F_m to assess the quenching level of IVF^B.

The temperature or nutrient dependence of NPQ effects on IVF^B was not experimentally assessed in this study. Temperature is a critical factor that determines the rates of enzymatic reactions (52), including the reactions for photosynthetic carbon fixation (53). The enhanced carbon fixation with increasing temperature can lower the excitation pressure (54), thereby reducing NPQ effects upon IVF^B. We propose that this phenomenon could be simulated by the ConFID model (see Appendix S10). The simulation showed that IVF^B negatively correlated with temperature (Figure S8), and the coefficient of temperature correction (see Appendix S10) was estimated to be −0.010 $°C^{-1}$, similar to the

literature value (14). And no interaction between effects of temperature and NPQ on IVF^B was found in the model experiment (Figure S8). Nutrient addition to a nutrient-limited or nutrient-starved culture can cause a fluorescence transience followed by recovery, but the direction of change will be different depending upon which nutrient is added—it could rise with nitrate enrichment but drop with ammonium or phosphate addition (15).

Comments and recommendations

In vivo fluorometry is a powerful and easy-to-use method for estimating phytoplankton Chl*a*. The enormous amount of IVF data, measured by ships, buoys and robots, have yielded an environmental treasure worth a great effort to understand and utilize. Multiple factors can, however, interfere with the method's accuracy. Our research focused on studying NPQ effects among others, and the results revealed as much as 50% decrease in the IVF^B is attributable to NPQ. We noted that NPQ-derived inaccuracies are to be expected during the main growing seasons of April–October in Long Island Sound, as an example of a highly-productive, temperate estuary (see Appendix S2). Vismann *et al.* (26) used *in vivo* fluorometry to monitor the amount of phytoplankton consumed by bivalve mollusks in the Limfjord, Denmark. They found a decreasing trend of IVF^B in the ambient water without bivalve feeding. The consumption rate of bivalves could not be accurately calculated without correcting for the NPQ effects. Li *et al.* (6) monitored the diel change of IVF^B in the Great Peconic Bay, New York, USA. That study documented a "U" shape similar to our Fig. 1, and the maximal decline was about 30%. The study in the Harpswell Sound, Maine, USA, observed a decrease of up to 80% (4). To correct for NPQ effects, simple equations have been introduced in this study. The compensating modeling equations were formulated upon the nature of NPQ; however, the representativeness of their coefficients needs to be evaluated in the future when IVF^B and light data from diverse environments were available. If the models with known coefficients fail to produce reasonable results, the process to derive correction models should be repeated. Changed coefficients will reflect spatial and temporal variabilities in environmental factors and dominant diatoms species or use of different models and/or brands of *in situ* fluorometers. For the latter, this study proposed a mathematical approach to model the I_{ex}-dependent NPQ effects on IVF^B which could be adjusted accordingly, and this advance may save substantial labor and time in the future. In general, although the correction efforts are far from straightforward, as demonstrated above, they are plausible to increase the level of confidence one should expect from environmental *in vivo* fluorescence data.

Acknowledgements—We thank NOAA Office of Aquaculture for funding the project. National Research Council hosted Yuyuan Xie's postdoctoral fellowship. University of California at San Barbara's analytic lab of the Marine Science Institute performed the nutrient analysis. We thank the anonymous reviewer for the constructive comments which improved the manuscript.

SUPPORTING INFORMATION

Additional supporting information may be found online in the Supporting Information section at the end of the article:

Appendix S1. Incubation light condition.

Appendix S2. Estimates of the mean, midday photosynthetically available radiation of the mixed layer in the Long Island Sound.

Appendix S3. Analysis of Chla, cell density, and nutrients.

Appendix S4. IVF data processing: temperature correction and cross-calibration.

Appendix S5. FIRe analysis procedure.

Appendix S6. Analysis of NPQ components.

Appendix S7. Discussion about triplet quenching.

Appendix S8. Fluorescence-chlorophyll Inversion for Diurnal cycle (ConFID) model.

Appendix S9. Additional results.

Appendix S10. Temperature dependence of NPQ effects on IVFB.

REFERENCES

1. Lorenzen (1966) A method for the continuous measurement of *in vivo* chlorophyll concentration. *Deep Sea Research* **13**, 223–227.
2. Mignot, A., H. Claustre, J. Uitz, A. Poteau, F. D'Ortenzio and X. Xing (2014) Understanding the seasonal dynamics of phytoplankton biomass and the deep chlorophyll maximum in oligotrophic environments: A bio-Argo float investigation. *Global Biogeochem. Cycles* **28**, 856–876.
3. Oviatt, C., L. Smith, J. Krumholz, C. Coupland, H. Stoffel, A. Keller, M. C. McManus and L. Reed (2017) Managed nutrient reduction impacts on nutrient concentrations, water clarity, primary production, and hypoxia in a north temperate estuary. *Estuar. Coast. Shelf Sci.* **199**, 25–34.
4. Carberry, L., C. Roesler and S. Drapeau (2019) Correcting in situ chlorophyll fluorescence time-series observations for nonphotochemical quenching and tidal variability reveals nonconservative phytoplankton variability in coastal waters. *Limnol Oceanogr Methods* **17**, 462–473.
5. Hall, N. S., A. C. Whipple and H. W. Paerl (2015) Vertical spatio-temporal patterns of phytoplankton due to migration behaviors in two shallow, microtidal estuaries: Influence on phytoplankton function and structure. *Estuar. Coast. Shelf Sci.* **162**, 7–21.
6. Li, Y., S. L. Meseck, M. S. Dixon, K. Rivara and G. H. Wikfors (2012) Temporal variability in phytoplankton removal by a commercial, suspended eastern oyster nursery and effects on local plankton dynamics. *J. Shellfish. Res.* **31**, 1077–1089.
7. Lucius, M. A., K. E. Johnston, L. W. Eichler, J. L. Farrell, V. W. Moriarty and R. A. Relyea (2020) Using machine learning to correct for nonphotochemical quenching in high-frequency, in vivo fluorometer data. *Limnology and Oceanography: Methods* **18**, 477–494.
8. Roesler, C., J. Uitz, H. Claustre, E. Boss, X. Xing, E. Organelli, N. Briggs, A. Bricaud, C. Schmechtig, A. Poteau, F. D'Ortenzio, J. Ras, S. Drapeau, N. Haëntjens and M. Barbieux (2017) Recommendations for obtaining unbiased chlorophyll estimates from in situ chlorophyll fluorometers: A global analysis of WET labs ECO sensors. *Limnology and Oceanography: Methods* **15**, 572–585.
9. Lawrenz, E. and T. L. Richardson (2010) How does the species used for calibration affect chlorophyll a measurements by in situ fluorometry? *Estuaries and Coasts* **34**, 872–883.
10. Alpine, A. E. and J. E. Cloern (1985) Differences in in vivo fluorescence yield between three phytoplankton size classes. *J. Plankton Res.* **7**, 381–390.
11. Xing, X., H. Claustre, S. Blain, F. D'Ortenzio, D. Antoine, J. Ras and C. Guinet (2012) Quenching correction for in vivo chlorophyll fluorescence acquired by autonomous platforms: A case study with instrumented elephant seals in the Kerguelen region (Southern Ocean). *Limnology and Oceanography: Methods* **10**, 483–495.
12. Rousso, B. Z., E. Bertone, R. A. Stewart, K. Rinke and D. P. Hamilton (2021) Light-induced fluorescence quenching leads to errors in sensor measurements of phytoplankton chlorophyll and phycocyanin. *Water Res.* **198**, 117133.
13. Liu, X. and A. P. Georgakakos (2021) Chlorophyll a estimation in lakes using multi-parameter sonde data. *Water Res.* **205**, 117661.

14. Watras, C. J., K. A. Morrison, J. L. Rubsam, P. C. Hanson, A. J. Watras, G. D. LaLiberte and P. Milewski (2017) A temperature compensation method for chlorophyll and phycocyanin fluorescence sensors in freshwater. *Limnology and Oceanography: Methods* **15**, 642–652.
15. Shelly, K., D. Holland and J. Beardall (2010) Assessing nutrient status of microalgae using chlorophyll a fluorescence. *Chlorophyll a Fluorescence in Aquatic Sciences: Methods and Applications*, **4**, 223–235.
16. Zaks, J., K. Amarnath, D. M. Kramer, K. K. Niyogi and G. R. Fleming (2012) A kinetic model of rapidly reversible nonphotochemical quenching. *Proc. Natl. Acad. Sci. U. S. A.* **109**, 15757–15762.
17. Lavaud, J., B. Rousseau and A.-L. Etienne (2004) General features of photoprotection by energy dissipation in planktonic diatoms (Bacillariophyceae). *J. Phycol.* **40**, 130–137.
18. Goss, R., E. Ann Pinto, C. Wilhelm and M. Richter (2006) The importance of a highly active and ΔpH-regulated diatoxanthin epoxidase for the regulation of the PS II antenna function in diadinoxanthin cycle containing algae. *J. Plant Physiol.* **163**, 1008–1021.
19. Nelson, D. M., P. Tréguer, M. A. Brzezinski, A. Leynaert and B. Quéguiner (1995) Production and dissolution of biogenic silica in the ocean: Revised global estimates, comparison with regional data and relationship to biogenic sedimentation. *Global Biogeochem. Cycles* **9**, 359–372.
20. Roegner, G. C., C. Seaton and A. M. Baptista (2010) Climatic and tidal forcing of hydrography and chlorophyll concentrations in the Columbia River estuary. *Estuaries and Coasts* **34**, 281–296.
21. Koh, C. H., J. S. Khim, H. Araki, H. Yamanishi, H. Mogi and K. Koga (2006) Tidal resuspension of microphytobenthic chlorophyll a in a Nanaura mudflat, Saga, Ariake Sea, Japan: Flood–ebb and spring–neap variations. *Mar. Ecol. Prog. Ser.* **312**, 85–100.
22. Thomalla, S. J., W. Moutier, T. J. Ryan-Keogh, L. Gregor and J. Schütt (2018) An optimized method for correcting fluorescence quenching using optical backscattering on autonomous platforms. *Limnology and Oceanography: Methods* **16**, 132–144.
23. Roesler, C. S. and A. H. Barnard (2013) Optical proxy for phytoplankton biomass in the absence of photophysiology: Rethinking the absorption line height. *Meth. Oceanograph.* **7**, 79–94.
24. Lee, J. H. W., I. J. Hodgkiss, K. T. M. Wong and I. H. Y. Lam (2005) Real time observations of coastal algal blooms by an early warning system. *Estuar. Coast. Shelf Sci.* **65**, 172–190.
25. Scheinin, M. and E. Asmala (2020) Ubiquitous patchiness in chlorophyll a concentration in coastal archipelago of Baltic Sea. *Front. Marine Sci.* **7**, 563.
26. Vismann, B., M. Wejlemann Holm, J. K. Davids, P. Dolmer, M. F. Pedersen, E. Blanda, H. T. Christensen, P. Nielsen and B. W. Hansen (2016) Field clearance of an intertidal bivalve bed: Relative significance of the co-occurring blue mussel Mytilus edulis and Pacific oyster Crassostrea gigas. *Aquat. Biol.* **25**, 107–119.
27. Falkowski, P. and D. A. Kiefer (1985) Chlorophyll a fluorescence in phytoplankton: Relationship to photosynthesis and biomass. *J. Plankton Res.* **7**, 715–731.
28. Maxwell, K. and G. N. Johnson (2000) Chlorophyll fluorescence--a practical guide. *J. Exp. Bot.* **51**, 659–668.
29. Morrison, J. R. (2003) In situ determination of the quantum yield of phytoplankton chlorophyll a fluorescence: A simple algorithm, observations, and a model. *Limnol. Oceanogr.* **48**, 618–631.
30. Mauzerall, D. (1978) Multiple excitations and the yield of chlorophyll a fluorescence in photosynthetic systems. *Photochem. Photobiol.* **28**, 991–998.
31. Kolber, Z. S., O. Prášil and P. G. Falkowski (1998) Measurements of variable chlorophyll fluorescence using fast repetition rate techniques: Defining methodology and experimental protocols. *Biochimica et Biophysica Acta (BBA) - Bioenergetics* **1367**, 88–106.
32. Gorbunov, M., Shirsin, E., Nikonova, E., Fadeev, V., & Falkowski, P. (2020). A multi-spectral fluorescence induction and relaxation (FIRe) technique for physiological and taxonomic analysis of phytoplankton communities. *Mar Ecol Prog Ser.* **644**, 1–13. https://doi.org/10.3354/meps13358
33. Schimanski, J., M. Beutler, C. Moldaenke and U. P. Hansen (2006) A model for correcting the fluorescence signal from a free-falling depth profiler. *Water Res.* **40**, 1616–1626.
34. Schuback, N. and P. D. Tortell (2019) Diurnal regulation of photosynthetic light absorption, electron transport and carbon fixation in two contrasting oceanic environments. *Biogeosciences* **16**, 1381–1399.
35. Xu, K., J. Lavaud, R. Perkins, E. Austen, M. Bonnanfant and D. A. Campbell (2018) Phytoplankton σPSII and excitation dissipation; implications for estimates of primary productivity. *Front. Marine Sci.* **5**, 281.
36. Serodio, J. and J. Lavaud (2011) A model for describing the light response of the nonphotochemical quenching of chlorophyll fluorescence. *Photosynth. Res.* **108**, 61–76.
37. Lepetit, B., G. Gelin, M. Lepetit, S. Sturm, S. Vugrinec, A. Rogato, P. G. Kroth, A. Falciatore and J. Lavaud (2017) The diatom Phaeodactylum tricornutum adjusts nonphotochemical fluorescence quenching capacity in response to dynamic light via fine-tuned Lhcx and xanthophyll cycle pigment synthesis. *New Phytol.* **214**, 205–218.
38. Cremella, B., Y. Huot and S. Bonilla (2018) Interpretation of total phytoplankton and cyanobacteria fluorescence from cross-calibrated fluorometers, including sensitivity to turbidity and colored dissolved organic matter. *Limnol. Oceanograph. Meth.* **16**, 881–894.
39. Murphy, C. D., G. Ni, G. Li, A. Barnett, K. Xu, J. Grant-Burt, J. D. Liefer, D. J. Suggett and D. A. Campbell (2017) Quantitating active photosystem II reaction center content from fluorescence induction transients. *Limnol. Oceanograph. Meth.* **15**, 54–69.
40. Giovagnetti, V., S. Flori, F. Tramontano, J. Lavaud and C. Brunet (2014) The velocity of light intensity increase modulates the photoprotective response in coastal diatoms. *PLoS One* **9**, e103782.
41. McKew, B. A., P. Davey, S. J. Finch, J. Hopkins, S. C. Lefebvre, M. V. Metodiev, K. Oxborough, C. A. Raines, T. Lawson and R. J. Geider (2013) The trade-off between the light-harvesting and photoprotective functions of fucoxanthin-chlorophyll proteins dominates light acclimation in *Emiliania huxleyi* (clone CCMP 1516). *New Phytol.* **200**, 74–85.
42. Han, B. P. (2000) Effect of photoinhibition on algal photosynthesis: A dynamic model. *J. Plankton Res.* **22**, 865–885.
43. Buck, J. M., J. Sherman, C. R. Bartulos, M. Serif, M. Halder, J. Henkel, A. Falciatore, J. Lavaud, M. Y. Gorbunov, P. G. Kroth, P. G. Falkowski and B. Lepetit (2019) Lhcx proteins provide photoprotection via thermal dissipation of absorbed light in the diatom Phaeodactylum tricornutum. *Nat. Commun.* **10**, 4167.
44. Long, S. P., S. Humphries and P. G. Falkowski (1994) Photoinhibition of photosynthesis in nature. *Annu. Rev. Plant. Physiol. Plant. Mol. Biol.* **45**, 633–662.
45. Schallenberg, C., R. F. Strzepek, N. Schuback, L. A. Clementson, P. W. Boyd and T. W. Trull (2020) Diel quenching of Southern Ocean phytoplankton fluorescence is related to iron limitation. *Biogeosciences* **17**, 793–812.
46. Beutler, M., K. H. Wiltshire, B. Meyer, C. Moldaenke, C. Luring, M. Meyerhofer, U. P. Hansen and H. Dau (2002) A fluorometric method for the differentiation of algal populations in vivo and in situ. *Photosynth. Res.* **72**, 39–53.
47. Campbell, D. A. and E. Tyystjärvi (2012) Parameterization of photosystem II photoinactivation and repair. *Biochim. Biophys. Acta - Bioenergetics* **1817**, 258–265.
48. Edwards, K. F., M. K. Thomas, C. A. Klausmeier and E. Litchman (2015) Light and growth in marine phytoplankton: Allometric, taxonomic, and environmental variation. *Limnol. Oceanogr.* **60**, 540–552.
49. Schwaderer, A. S., K. Yoshiyama, P. de Tezanos Pinto, N. G. Swenson, C. A. Klausmeier and E. Litchman (2011) Eco-evolutionary differences in light utilization traits and distributions of freshwater phytoplankton. *Limnol. Oceanogr.* **56**, 589–598.
50. Lepetit, B., R. Goss, T. Jakob and C. Wilhelm (2012) Molecular dynamics of the diatom thylakoid membrane under different light conditions. *Photosynth. Res.* **111**, 245–257.
51. Grouneva, I., T. Jakob, C. Wilhelm and R. Goss (2008) A new multicomponent NPQ mechanism in the diatom Cyclotella meneghiniana. *Plant Cell Physiol.* **49**, 1217–1225.
52. Raven, J. A. and R. J. Geider (1988) Temperature and algal growth. *New Phytol.* **110**, 441–461.
53. Li, W. K. W., J. C. Smith and T. Platt (1984) Temperature response of photosynthethic capacity and carboxylase activity in Arctic marine phytoplankton. *Mar. Ecol. Prog. Ser.* **17**, 237–243.
54. Maxwell, D. P., S. Falk and N. Huner (1995) Photosystem II excitation pressure and development of resistance to photoinhibition (I. light-harvesting complex II abundance and zeaxanthin content in Chlorella vulgaris). *Plant Physiol.* **107**, 687–694.